International Journal
of Micro Air Vehicles

ORIGINAL RESEARCH ARTICLE

Open Access

https://doi.org/10.48130/mav-0026-0012

*International Journal of Micro Air Vehicles* **2026**, 18: e012

# Affine formation maneuver control for gate-traversing drone swarms: algorithm and application

Peng Yi[1], Junming Xie[1], Wei Yu[2], Bo Zhu[3*], Tianjiang Hu[1*] and Deqing Huang[4]

[1] *School of Aeronautics and Astronautics, Sun Yat-sen University, Guangzhou, Guangdong 510725, China*
[2] *Faculty of Data Science, City University of Macau, Macau SAR China 999078, China*
[3] *School of Robotics and Automation, Nanjing University, Suzhou, Jiangsu 215163, China*
[4] *School of Electrical Engineering, Southwest Jiaotong University, Chengdu, Sichuan 611756, China*
* Correspondence: zhubo@nju.edu.cn (Zhu B); hutj3@mail.sysu.edu.cn (Hu T)

## Abstract

While recent advancements in affine formation control have demonstrated that leveraging historical information can enhance swarm performance without altering network topology, bridging the gap between theoretical models and practical, complex spatial maneuvers remains a significant challenge. To address this, this paper investigates the maneuver control problem for a quadrotor swarm navigating through constrained environments, specifically gate-traversing scenarios. Unlike existing literature that primarily focuses on follower tracking, we simultaneously address the planning and control problems for both leader and follower agents. First, we develop a hierarchical framework incorporating planning strategies for formation rotation and scaling to accommodate spatial gate variations and onboard visual perception constraints. Furthermore, to significantly enhance maneuver cohesiveness and overall traversability, we propose a distributed formation tracking controller for followers that innovatively integrates historical horizontal velocity commands (HHVC) and historical vertical acceleration commands (HVAC). The efficacy of the proposed approach is comprehensively validated through numerical simulations and real-world experiments using a swarm of seven DJI Tello quadrotors. The results demonstrate that the swarm successfully traverses multiple gates with diverse heights and orientations, exhibiting superior responsiveness, smoother trajectories, and improved formation cohesiveness.

**Keywords:** Affine formation control, Drone swarm, Maneuver control, Historical command, Cohesiveness

**Citation:** Yi P, Xie J, Yu W, Zhu B, Hu T, et al. 2026. Affine formation maneuver control for gate-traversing drone swarms: algorithm and application. *International Journal of Micro Air Vehicles* 18: e012 https://doi.org/10.48130/mav-0026-0012

## Introduction

Swarm robotics has garnered growing scholarly interest in recent years due to its vast potential for applications in collaborative tasks, including exploration[1], inspection[2], and search-and-rescue[3]. The affine formation control methodology for swarm systems has garnered attention due to its advantages of 'regulating a multitude of followers with a minimal number of leaders' and its support for various maneuver behaviors[4].

The theoretical foundations for affine formation were established in the previous research[5], which delineated the necessary and sufficient conditions for formation realization through graph-theoretic analysis. Zhao[6] developed control laws to track any target formation that is a time-varying affine transformation of a nominal configuration. A hierarchical affine control algorithm, introduced in an existing study[7], is capable of achieving formation control under partial information constraints.

Recently, affine formation control has garnered significant academic attention due to its flexibility in maneuvers. However, existing literature frequently overlooks the coupled planning problem in constrained environments, which is crucial for real-world deployments. Wang et al.[8] addressed the prescribed-time affine formation control problem for multi-agent systems. Xiao et al.[9] investigated topology design and leader selection strategies, and proposed an approach to optimize the stress matrix for efficient communication, rapid convergence, and time-delay tolerance. Yu et al.[10,11] introduced the historical commands to improve the system cohesiveness.

For traversing tasks, most research focuses on the individual UAV. Wang et al.[12] adapted the framework of model predictive contouring control for high-speed path-following control applications to address the limitations of the effective sensing range of onboard sensors. Bonatti et al.[13] proposed a novel method for learning robust visuomotor policies that can be trained purely with simulated data. Cyba et al.[14] introduced two innovative control strategies designed for autonomous drone racing.

Departing from the works on traversal capabilities of individual UAVs, this paper emphasizes the traversal capability of drone swarms across different gates. This shift introduces several challenges: (i) adaptation: the dynamic formation configurations in response to gates at different heights and orientations; (ii) excellent maneuver control performance: ensuring rapid convergence to the desired configuration while maintaining strong cohesiveness; and (iii) safety: collision-free maneuver.

To address these challenges, we propose an effective planning and control algorithm for drone swarms traversing narrow areas. The core idea involves transforming the problem of swarm formation traversal into a hierarchical design problem within the leader-follower framework. In general, we simplify the planning of the entire swarm's traversal formation into two key components: (i) the traversal planning of leader drones; and (ii) the control of follower drones with enhanced cohesiveness. Specifically, we analyze the dynamic constraints imposed by the environment on the leader configuration and design a maneuver control to ensure the safe traversal of leader drones. Additionally, by constructively incorporating historical information into the formation controller of followers, we improve the transient performance of the follower formation

https://doi.org/10.48130/mav-0026-0012

maneuver while maintaining system stability. Through the decoupling and hierarchical design, we significantly reduce the computational complexity of swarm planning, thereby enhancing the adaptability and robustness of UAV swarms in complex environments. Our key contributions are:

(1) We simultaneously address the planning and control problems for leader and follower quadrotors. This is different from most existing works on affine formation maneuver control where only the control problem of followers is concerned. More specifically, taking into account the gate-traversing scenario and constraints of onboard visual perception, we develop planning strategies for both traversal direction and formation configuration. By considering both horizontal and altitude maneuvers, this control scheme enables 3D spatial (rather than just 2D) formation maneuvers.

(2) Unlike conventional affine formation protocols that rely solely on instantaneous states, we propose a novel distributed control law augmented with Historical Horizontal Velocity Commands (HHVC) and Historical Vertical Acceleration Commands (HVAC). This integration is specifically designed to counteract the inherent underactuated dynamics of quadrotors, thereby significantly enhancing maneuver cohesiveness and traversability when the swarm executes aggressive spatial reconfigurations to navigate through sequential narrow gates. The term *cohesiveness performance* refers to the synchronization of a formation's transition from its current state to a target configuration[15]. In recent years, in fields of biological swarm behavior, physics, and robotic swarm control, researchers have discovered that leveraging historical or memory information can enhance the cohesiveness of swarm systems[10,11,16,17].

(3) We implement the planning and control solutions on a swarm of 7 DJI Tello quadrotors. We consider the task of traversing three gates with diverse vertical and horizontal configurations. Simulation and experimental case studies are performed to verify the performance improvement. The comparison results have demonstrated that, compared to the results of the basic affine scale formation maneuvering algorithm[18], our algorithm ensures significant improvements in system responsiveness, smoothness, cohesiveness, and traversability.

# Preliminaries and problem formulation

Consider a group of $n$ UAVs with $n_l$ leaders and $n_f$ followers in $\mathbb{R}^d$, where $d \geq 2$ and $n = n_l + n_f > d+1$. A *configuration* of $n$ UAVs is defined by their coordinates $\{p\}_{i=1}^n$ in Euclidean space $\mathbb{R}^d$, denoted as $p = [p_1^T, \ldots, p_n^T] = [p_l^T, p_f^T] \in \mathbb{R}^{d\times n}$, where $p_l$ and $p_f$ denote the coordinates of leaders and followers respectively. Besides, the *configuration matrix* $P \in \mathbb{R}^{n\times d}$ and *augmented configuration matrix* $\overline{P} \in \mathbb{R}^{n\times(d+1)}$ are defined as:

$$P(p) = \begin{bmatrix} p_1^T \\ \vdots \\ p_n^T \end{bmatrix}, \overline{P}(p) = \begin{bmatrix} p_1^T & 1 \\ \vdots & \vdots \\ p_n^T & 1 \end{bmatrix} = [P, \mathbf{1}_n]. \tag{1}$$

The *affine span* of set $\{p_i\}_{i=1}^n$ is defined as:

$$\mathcal{S} = \left\{ \sum_{i=1}^n a_i p_i : u_i \in \mathbb{R} \text{ for all } i \text{ and } \sum_{i=1}^n a_i = 1 \right\}, \tag{2}$$

where, $a_i$ is a scalar. Based on the work by Zhao[6], the set of points $\{p_i\}_{i=1}^n$ affinely span $\mathbb{R}^d$ if and only if $n \geq d+1, \mathrm{rank}(\overline{P}) = d+1$.

Given a constant set of points $\{r_i\}_{i=1}^n$, the *nominal configuration* is defined as $r = [r_1^T, \ldots, r_n^T] = [r_l^T, r_f^T] \in \mathbb{R}^{n\times d}$. The following *affine image* defined in the study by Lin et al.[5] is employed here:

$$\mathcal{A}(r) = \Big\{ q = [q_1^T, \cdots q_2^T] \in \mathbb{R}^{d\times n} : q_i = Ar_i + b, \\ A \in \mathbb{R}^{d\times d} \text{ and } b \in \mathbb{R}^d, i = 1, \ldots, n \Big\}, \tag{3}$$

where, $(A, b)$ represents an operator for *affine transformation*, for instance, a translation, rotation, scaling, shear, etc.

To describe the connection among UAVs, we consider an undirected graph $\mathcal{G} = (\mathcal{V}, \mathcal{E})$ consists of a node set $\mathcal{V} = \{v_1, \ldots, v_n\}$ and an edge set $\mathcal{E} \in \mathcal{V}\times\mathcal{V}$. To distinguish different types of UAV nodes, we define $\mathcal{V} = [\mathcal{V}_l, \mathcal{V}_f]$, where $\mathcal{V}_l = [v_1, \ldots, v_l]$ and $\mathcal{V}_f = [v_{l+1}, \ldots, v_f]$. An edge $(i, j)$ means that UAV $i$ and UAV $j$ communicate with each other. The set of neighbors of UAV $i$ is defined as $\mathcal{N}_i = \{j \in \mathcal{V} | (i, j) \in \mathcal{E}, i \neq j\}$. A formation is the graph $\mathcal{G}$ with vertices $\{i\}_{i=1}^n$ mapped to a point set $\{p_i\}_{i=1}^n$ and denoted as $(\mathcal{G}, p)$.

To describe the universal rigidity of a formation, the concept of stress[19], is reviewed in this paper. For a formation $(\mathcal{G}, p)$, we apply a positive or negative weight scalar $\omega_{ij} = \omega_{ji}$ to all edges $(i, j)$ of the formation. The set of the weight $\{\omega_{ij}\}_{(i,j)\in\mathcal{E}}$ is denoted as a *stress* of $(\mathcal{G}, p)$. Given a configuration $p^*$, a stress is called *equilibrium stress* of $(\mathcal{G}, p^*)$ if it satisfies $\sum_{j\in\mathcal{N}_i} \omega_{ij}(p_j^* - p_i^*) = 0, \forall j \in \mathcal{V}$. The *stress matrix* $\Omega \in \mathbb{R}^d$ is the matrix form of equilibrium stress, expressed as:

$$[\Omega]_{ij} = \begin{cases} -\omega_{ij}, & i \neq j, j \in \mathcal{N}_i, \\ 0, & i \neq j, j \notin \mathcal{N}_i, \\ \sum_{k\in\mathcal{N}_i} \omega_{ik}, & i = j. \end{cases} \tag{4}$$

Meanwhile, define

$$\overline{\Omega} = \Omega \otimes I_d = \begin{bmatrix} \overline{\Omega}_{ll} & \overline{\Omega}_{lf} \\ \overline{\Omega}_{fl} & \overline{\Omega}_{ff} \end{bmatrix}, \tag{5}$$

where, $\otimes$ denotes Kronecker product, $I_d$ denotes $d\times d$ identity matrix, $\overline{\Omega}_{ll} \in \mathbb{R}^{(dn_l)\times(dn_l)}$, $\overline{\Omega}_{lf} \in \mathbb{R}^{(dn_l)\times(dn_f)}$, $\overline{\Omega}_{fl} \in \mathbb{R}^{(dn_f)\times(dn_l)}$ and $\overline{\Omega}_{ff} \in \mathbb{R}^{(dn_f)\times(dn_f)}$.

Two lemmas regarding the universal rigidity and the problem of leader selection are introduced.

**Lemma 1** *(Lemma 2[6]) A formation $(\mathcal{G}, p)$ is universally rigid if a related positive semidefinite stress matrix $\Omega$ exists and satisfies* $\mathrm{rank}(\Omega) = n - d - 1$.

**Lemma 2** *(Theorem 2[6]) For a given nominal formation $(\mathcal{G}, r)$, if the set of $\{r_i\}_{i\in\mathcal{V}_l}$ affinely spans in $\mathbb{R}^d$, then followers' coordinates $p_f$ can be uniquely determined by leaders' coordinates $p_l$ as $p_f = -\overline{\Omega}_{ff}^{-1}\overline{\Omega}_{fl}p_l$.*

**Assumption 1** *The nominal formation $(\mathcal{G}, r)$ is universally rigid, and the set of points $\{r_i\}_{i=1}^n$ affinely spans $\mathbb{R}^d$.*

**Remark 1** *Intuitively, universal rigidity ensures that the formation's shape is uniquely determined by the inter-agent distances. Meanwhile, a universally rigid formation guarantees that during formation maneuvers, no subset of agents can move independently while the rest remain fixed, preventing geometric ambiguities. The affine spanning condition ensures that the agents occupy the full d-dimensional space, so the formation is non-degenerate and can perform all required translations, rotations, and shape transformations.*

Meanwhile, we define the formation error as:

$$\epsilon_{(i,j)} = \omega_{ij}(p_i - p_j), (i, j) \in \mathcal{E}. \tag{6}$$

Motivated by Devasia[15], we define the metric to assess the cohesiveness of affine formation as follows:

$$\Delta_f = \frac{1}{T_s} \int_0^{T_s} |e_f(t) - \overline{e}(t)\mathbf{1}_f|_1 \, \mathrm{d}t, \tag{7}$$

where, $T_s$ is the settling time. $|\cdot|_1$ is the standard vector 1-norm, $e_f(t) = [\epsilon_1(t), \ldots, \epsilon_f(t)]^T, \epsilon_i = \sum_{j\in\mathcal{N}_i} \omega_{ij}(p_i - p_j), i \in \mathcal{V}_f$ and $\overline{e}(t) = 1/f \sum_{i=1}^f \epsilon_i(t), i \in \mathcal{V}_f$ denotes the average value of error $\epsilon_i$.

**Remark 2** *The metric $\Delta_f$ quantifies the dynamic cohesiveness of a formation during a maneuver. Physically, it measures how similarly the individual UAVs converge to the desired formation over time: a smaller $\Delta_f$ indicates that the UAVs remain closely coordinated, maintaining their relative positions and velocities throughout the transition. Conversely, a larger $\Delta_f$ reflects greater divergence among UAVs during the maneuver, implying that some individuals lag behind or deviate from the formation. In essence, $\Delta_f$ captures the structural integrity of the formation as it evolves, providing a dynamic performance indicator beyond simply comparing the initial and final states.*

With the preliminaries, we proposed several controllers to enhance the traversability of a UAV swarm under the assumption of known traversable area information, which includes the width $W_T$, relative position of the center $P_{\text{relative}}$, and heading angle $\alpha_T$ of the area. The rationale for this assumption is supported by recent studies demonstrating that gate information, including size, relative orientation, and relative position, can be reliably obtained from onboard sensors such as cameras[20−22]. Based on this, the focus of this work is not on how the gate information is perceived, but rather on how it is effectively utilized to enable formation traversal through constrained areas. To evaluate the fast maneuverability and traversability challenges while considering the dynamic characteristics of copter drones, we strategically decouple the problem into horizontal and vertical dimensions for efficient analysis and implementation, as shown in Fig. 1.

Considering that most commercial quadrotors provide velocity and attitude autopilots as black boxes and exhibit stronger vertical than horizontal maneuverability, we model the UAVs with single-integrator dynamics in the horizontal plane (x-y) and double-integrator dynamics in the vertical direction (z):

$$\begin{aligned} \dot{p}_i^{xy} &= u_i^{xy}, i \in \mathcal{V}, \\ \ddot{p}_i^{z} &= u_i^{z}, i \in \mathcal{V}, \end{aligned} \tag{8}$$

where, $p_i^{xy} \in \mathbb{R}^2, p_i^z \in \mathbb{R}$ are the horizontal and vertical position of UAV $i$ and $u_i^{xy} \in \mathbb{R}^2, u_i^z \in \mathbb{R}$ denotes for the control input. Assume each UAV is represented as a node, and the interaction relationships among them are captured by the stress matrix. The target of horizontal formation is to design distributed control laws $u_i^{xy}, u_i^z, i \in \mathcal{V}$, such that

$$\lim_{t\to\infty}(p_i^{xy}(t) - p_j^{xy}(t)) = \kappa \cdot \boldsymbol{R}(p_i^{*xy}(t) - p_j^{*xy}(t)), \forall (i,j) \in \mathcal{E}, \tag{9}$$

$$\lim_{t\to\infty}(p_i^{z}(t) - p_j^{z}(t)) = (p_i^{*z}(t) - p_j^{*z}(t)), \forall (i,j) \in \mathcal{E}, \tag{10}$$

where, $\kappa$ is a positive scalar and denotes the scale command, $\boldsymbol{R} \in \mathbb{R}^{2\times 2}$ is the rotation matrix and denotes the formation rotation command.

This paper aims to enhance the traversability of UAV swarms across constrained areas. The traversability optimization is achieved by fully exploiting the roles of leaders in affine formation maneuvers. The cohesiveness of swarm systems is enhanced by using the memory control commands to construct current control commands for followers, motivated by the ideas mentioned in the study by Yu et al.[11] and Devasia[15].

# Methodology

In this section, differentiated traversability optimization strategies are proposed for both the leader UAVs and the follower UAVs in the formation, as illustrated in the proposed framework shown in Fig. 2.

In the proposed framework, UAVs are categorized as leader and follower roles with distinct responsibilities. Leader UAVs are

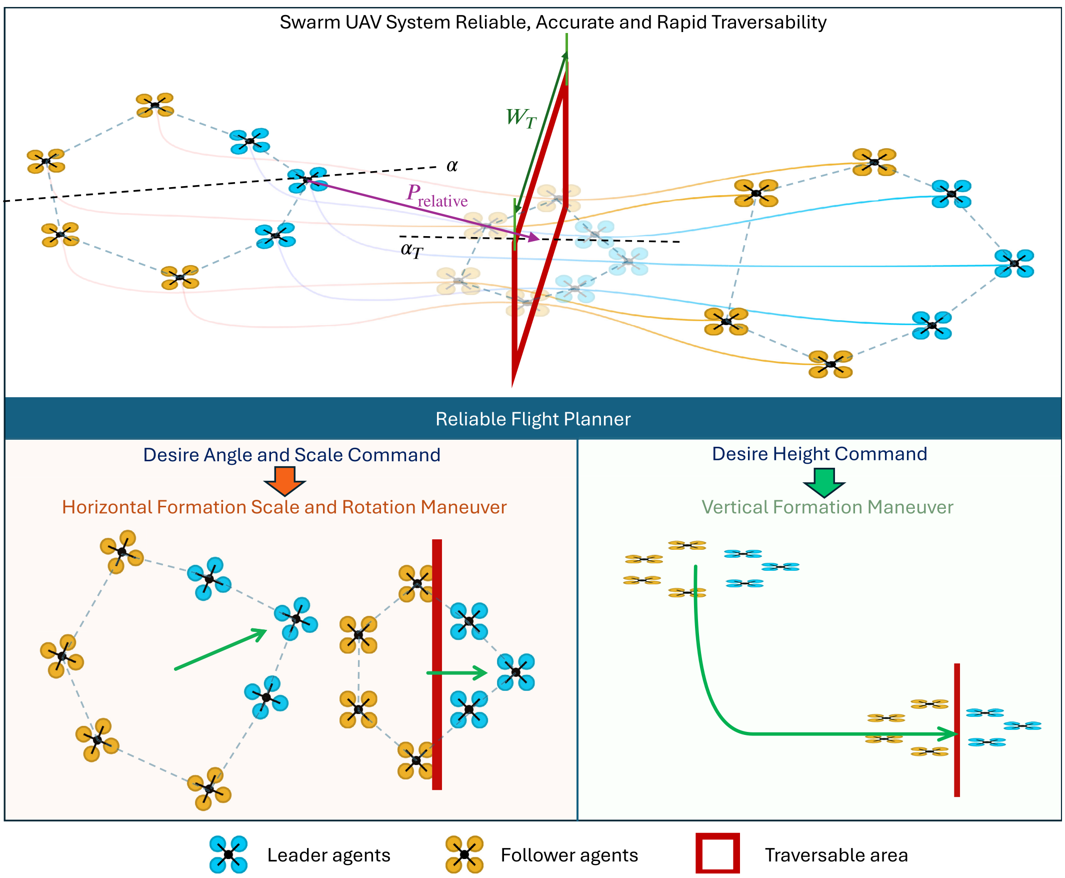


**Fig. 1** Diagram of a UAV swarm traversing problem.

https://doi.org/10.48130/mav-0026-0012

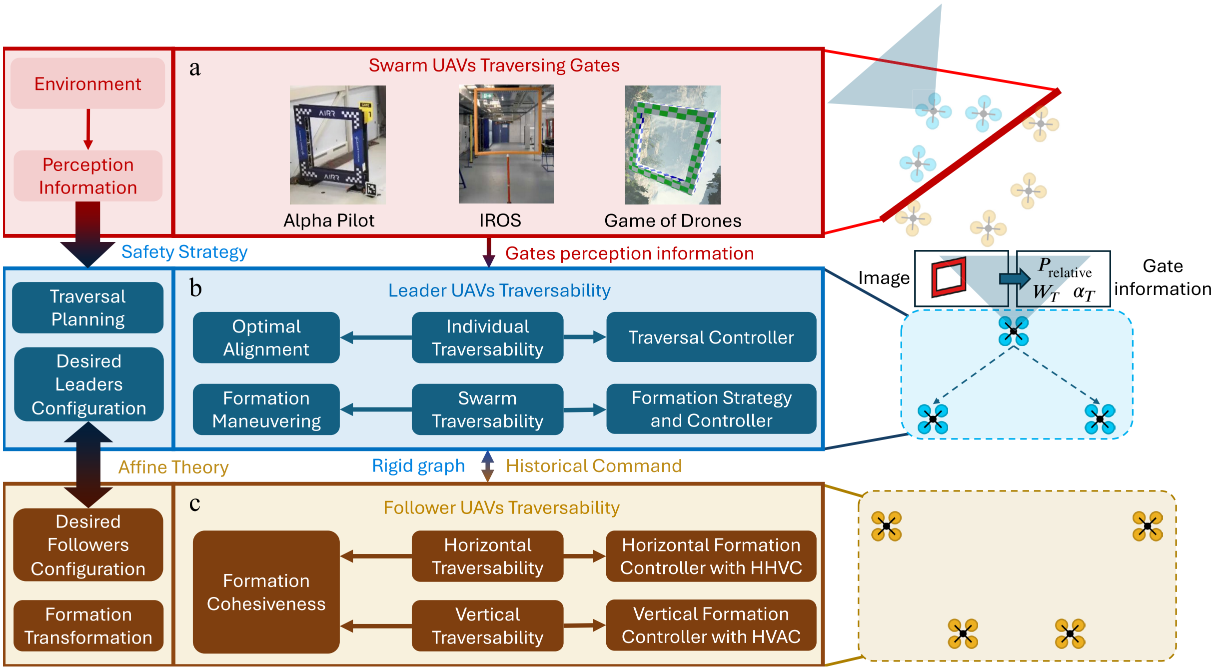


**Fig. 2** Diagram of a UAV swarm traversing framework.

assumed to have access to the necessary gate information, including width $W_T$, relative heading angle $\alpha_T$, and relative position $P_{\text{relative}}$. This information is necessary to generate safe traversal trajectories and determine formation configuration. Follower UAVs do not directly access the perception information; instead, they rely on the neighbor's historical control signals to maintain formation cohesion.

For leader UAVs, the optimization of traversability is approached through two distinct aspects. First, as the core decision-making units, the leader UAVs must exhibit superior individual traversability, primarily reflected in their ability to navigate swiftly through geometrically constrained areas using available perception information. Second, as formation leaders, they are responsible for dynamic reconfiguration of the formation. This requires computing formation parameters, including size and heading, based on the geometry of constrained areas.

For follower UAVs, traversability is largely contingent on the maintenance of formation cohesion. Followers must employ distributed collaborative control algorithms to promptly respond to the desired position, which is produced by the leaders' maneuvering in affine formation control. By continuously adjusting their position in real time, they preserve the structural cohesiveness of the formation configuration. This enables the dynamic adaptation of the formation, ultimately improving the overall traversability.

Based on the above analysis, we proposed a comprehensive controller as:

$$u_i^{xy} = \begin{cases} u_i^{t_{xy}} + u_i^{f_{xy}} + u_i^c, & i \in \mathcal{V}_l, \\ u_i^{f_{xy}} + u_i^c, & i \in \mathcal{V}_f, \end{cases} \qquad u_i^{z} = \begin{cases} u_i^{t_{z}}, & i \in \mathcal{V}_l, \\ u_i^{f_{z}}, & i \in \mathcal{V}_f, \end{cases} \tag{11}$$

where, $u_i^{t_{xy}}, u_i^{t_z}, i \in \mathcal{V}_l$ are the traversal control inputs for leaders based on target relative geometry to achieve optimal alignment with constrained areas, while rapid traversal $u_i^{f_{xy}}, i \in \mathcal{V}_l$ are the formation control input to adjust the subgraph of leaders with optimal traversable formation parameters. $u_i^{f_{xy}}, u_i^{f_z}, i \in \mathcal{V}_f$ are the formation control inputs for followers to promptly respond to the maneuvering of leaders and keep the formation cohesiveness. $u_i^c, i \in \mathcal{V}$ is the control input to avoid collision among UAVs.

## Formation tracking controllers for followers

Motivated by the ideas in our previous works[10,11], we introduce the historical command to enhance the system performance:

$$\begin{aligned} u_i^{f_{xy}}(t) = & -k_\omega^{xy} k_p^{xy} \sum_{(i,j)\in\mathcal{E}} \omega_{ij}[(p_i^{xy}(t) - p_j^{xy}(t))] \\ & -k_\omega^{xy} \sum_{(i,j)\in\mathcal{E}} \omega_{ij}[u_i^{f_{xy}}(t-\tau) - u_j^{f_{xy}}(t-\tau)] \\ & +u_i^{f_{xy}}(t-\tau), i \in \mathcal{V}_f, \end{aligned} \tag{12}$$

$$\begin{aligned} u_i^{f_z}(t) = & -k_\omega^z k_p^z \sum_{(i,j)\in\mathcal{E}} \omega_{ij}^z[(p_i^z(t) - p_j^z(t))] + u_i^{f_z}(t-\tau) \\ & -k_\omega^z k_v^z \sum_{(i,j)\in\mathcal{E}} \omega_{ij}^z[(\dot{p}_i^z(t) - \dot{p}_j^z(t))] \\ & -k_\omega^z \sum_{(i,j)\in\mathcal{E}} \omega_{ij}^z[u_i^{f_z}(t-\tau) - u_j^{f_z}(t-\tau)], i \in \mathcal{V}_f, \end{aligned} \tag{13}$$

where, $\tau = n * T, n \in \mathbb{N}^+$ denotes delay period, $T$ denotes the control period, and $k_p^z, k_v^z, k_p^{xy}$ are positive scalars.

**Lemma 3** *(Theorem 2[10]) The horizontal tracking error of followers are globally uniformly ultimately bounded with $\tau > 0$ if $k_\omega^{xy}$ is satisfied*

$$0 < k_\omega^{xy} < \min_{1 \le ff \le n_f} \left\{ \frac{2}{\lambda_{ff}^{xy}} \right\}, \tag{14}$$

*where, $\lambda_{ff}^{xy}$ is the eigenvalue of $\overline{\Omega}_{ff}^{xy}$.*

**Lemma 4** *(Theorem 1[11]) The vertical tracking error of followers are globally uniformly ultimately bounded with $\tau > 0$ if $k_\omega^z, k_p^z, k_v^z$ are satisfied*

$$\begin{cases} 0 < k_\omega^z < \min\limits_{1 \le ff \le n_f} \left\{ \dfrac{2}{\lambda_{ff}^z} \right\}, \\ \dfrac{k_v^{z2}}{k_p^z} > \max\limits_{1 \le ff \le n_f} \dfrac{2 - 2\sqrt{1 - (1 - k_\omega^z \lambda_{ff}^z)^2}}{k_\omega^z \lambda_{ff}^z}, \end{cases} \tag{15}$$

*where, $\lambda_{ff}^z$ is the eigenvalue of $\overline{\Omega}_{ff}^z$.*

## Design of formation controller for leaders

According to Lemma 2, the subgraph associated with $d+1$ pairs of leader UAVs are selected as $\mathcal{V}_l = \{v_1, \ldots, v_l\}$.

To guarantee the secure and reliable traversal of the entire swarm formation through traversable regions, a robust safety strategy is established to generate scaling and rotational commands, which are subsequently transmitted to the leaders.

(1) Scale command design:

$$\kappa = k_{\text{safe}}^{\kappa} \frac{W_T}{W^*}, \tag{16}$$

where, $k_{\text{safe}}^{\kappa} \in (\lambda_{\min}, 1)$ is a scalar, $W_T$ is the maximum traversable width and $W^* = \max_{i\in\mathcal{V}}\{p_i^{*y}\} - \min_{i\in\mathcal{V}}\{p_i^{*y}\}$ denotes the width of the nominal formation.

(2) Rotational command design:

For the purpose of smoother formation dynamics and the elimination of abrupt angular deviations, an intermediate auxiliary variable is introduced to optimize the robustness and continuity of rotational formation maneuvering. The rotational command is generated as:

$$\begin{cases} \dot{\alpha}_d = u_\alpha \leq 10\,\text{deg}/\text{s}, \\ u_\alpha = -k_p^{\alpha} \cdot (\alpha_d - \alpha_T), \end{cases} \tag{17}$$

where, $\alpha_T$ denotes the heading angle of the gate, $\alpha_d$ is the rotational angle command, and $k_p^{\alpha}$ is a positive scalar.

(3) Controller design:

To implement desire scale and rotation generated by the above strategies, the leader UAV's formation controller is designed as:

$$\begin{aligned} u_i^{f_{xy}} &= -k_\omega^{xy} \sum_{(i,j)\in\mathcal{E}} \omega_{ij}^{xy}(p_i^{xy} - p_j^{xy}) \\ &- k_\kappa \sum_{(i,j)\in\mathcal{E}_l} [(p_i^{xy} - p_j^{xy}) - \kappa \cdot \boldsymbol{R}(p_i^{*xy} - p_j^{*xy})], i \in \mathcal{V}_l, \end{aligned} \tag{18}$$

where, $p_i^{xy}, i \in \mathcal{V}$ denotes the horizontal position of UAV $i$, $\omega_{ij}^{xy}$ denotes the stress of edge $(i,j)$, $k_\omega^{xy}$ and $k_\kappa$ are positive scalars, $\kappa$ is the desire scale command generated by Eq. (16), $\boldsymbol{R} = \begin{bmatrix} \cos\alpha_d & -\sin\alpha_d \\ \sin\alpha_d & \cos\alpha_d \end{bmatrix}$, and $\alpha_d$ is desire rotation command generated by Eq. (17). The former entry of Eq. (18) means the internal force to keep the formation shape and imporve the cohesiveness, while the other one represents the external force to implement the formation scale and rotation.

**Theorem 1** *Under Assumption 1, the horizontal tracking error under controller* (12), (18) *are globally uniformly ultimately bounded.*

**Proof 1** *From Lemma 3, we have*

$$\lim_{t\to\infty} p_f^{xy} + \overline{\Omega}_{ff}^{xy\,-1} \overline{\Omega}_{fl}^{xy} p_l^{xy} = 0, \tag{19}$$

*where,* $p_l^{xy} = [p_1^{xyT}, \ldots, p_l^{xyT}]^T \in \mathbb{R}^{2n_l}$ *and* $p_f^{xy} = [p_{l+1}^{xy\,T}, \ldots, p_n^{xyT}]^T \in \mathbb{R}^{2n_f}$.

*For leaders, the controller* (12) *can be written as:*

$$u_l^{xy} = -\overline{\Omega}_{ll}^{xy} p_l^{xy} - \overline{\Omega}_{lf}^{xy} p_f^{xy} - \overline{\Omega}_{ll}^{xy} \tilde{p}_l^{xy}, \tag{20}$$

*where,* $\tilde{p}_l^{xy} = [\tilde{p}_1^{xyT}, \ldots, \tilde{p}_l^{xyT}] \in \mathbb{R}^{2n_l}$, *and* $\tilde{p}_i^{xy} \in \mathbb{R}^2$ *is defined as:*

$$\tilde{p}_i^{xy} = p_i^{xy} - \kappa \cdot \boldsymbol{R} p_i^{*xy}, i \in \mathcal{V}_l, \tag{21}$$

*by using the stress equilibrium condition that* $\overline{\Omega}_{ll}^{xy} p_l^{*xy} = 0$. *Then, the closed-loop error dynamics can be written as:*

$$\dot{\tilde{p}}_l^{xy} = -\overline{\Omega}_{ll}^{xy} p_l^{xy} - \overline{\Omega}_{lf}^{xy} p_f^{xy} - \overline{\Omega}_{ll}^{xy} \tilde{p}_l^{xy}, \tag{22}$$

*combining Eqs* (19) *and* (22), *we have*

$$\dot{\tilde{p}}_l^{xy} = -\overline{\Omega}_{ll}^{xy} \tilde{p}_l^{xy}. \tag{23}$$

*Note that the eigenva of this matrix always holds negative real part according to Lemma 1 and Assumption 1. Hence, the error globally exponentially converges to zero, which means*

$$\lim_{t\to\infty} p_l^{xy} = \kappa \cdot \boldsymbol{R} p_l^{*xy}. \tag{24}$$

*Thus, Eq.* (19) *can be written as:*

$$\lim_{t\to\infty} p_f^{xy} = -\kappa \cdot \boldsymbol{R} \overline{\Omega}_{ff}^{xy\,-1} \overline{\Omega}_{fl}^{xy} p_l^{*xy} = \kappa \cdot \boldsymbol{R} p_f^{*xy}. \tag{25}$$

*Based on the analysis presented above, we have*

$$\lim_{t\to\infty} p_i^{xy} = \kappa \cdot \boldsymbol{R} p_i^{*xy}, i \in \mathcal{V}. \tag{26}$$

## Traversal controller for leaders

To facilitate the design of the travel controller, we defined direction error $E_{\text{lateral}}$ and forward error $E_{\text{forward}}$ as:

$$\begin{aligned} E_{\text{forward}} &= \text{Proj}(E_T, \boldsymbol{n}) = \frac{E_t \cdot \boldsymbol{n}}{\|\boldsymbol{n}\|} \cdot \frac{\boldsymbol{n}}{\|\boldsymbol{n}\|}, \\ E_{\text{lateral}} &= E_T - E_{\text{forward}}, \end{aligned} \tag{27}$$

where, $E_T = P_{\text{relative}}$ denotes the position error between the leader UAV and the gate, $\|\cdot\|$ denotes the Euclidian norm of a vector, $\boldsymbol{n} = [\cos\tilde{\alpha}, \sin\tilde{\alpha}]$ is the normal vector of the constrained area and $\tilde{\alpha} = \alpha - \alpha_T$ is the angle difference between formation and the constrained area. From the error (27), the travel controller is designed as:

$$u_i^{t_{xy}} = k_f E_{\text{forward}} + k_d E_{\text{lateral}}, i \in \mathcal{V}_l. \tag{28}$$

Considering a dangerous case that leaders are seriously close to the traversable area but not aligned with the center of the area, shown as Fig. 3b, the controller is further improved as:

$$\begin{aligned} u_i^{t_{xy}} &= k_f \left[ E_{\text{forward}} - \|E_{\text{forward}}\| \cdot 2^{\left(1 - \frac{1}{d_{\text{safe}}} \cdot \frac{\|E_{\text{forward}}\|}{\|E_{\text{lateral}}\|}\right)} \cdot \boldsymbol{n} \right] \\ &+ k_d E_{\text{lateral}}, i \in \mathcal{V}_l, \end{aligned} \tag{29}$$

where, $d_{\text{safe}}$ is a positive scalar denoted as a safe distance. Note that, Eqs (29) and (28) exhibit approximate equivalence if $\|E_{\text{forward}}\| \gg \|E_{\text{lateral}}\|$.

Additionally, to achieve optimal alignment of the leader UAVs with the constrained area in the vertical dimension, the travel controller is designed as:

$$u_i^{t_z} = -k_{pl}^z \tilde{p}_i^z - k_{dl}^z \dot{p}_i^z, i \in \mathcal{V}_l, \tag{30}$$

where, $p_i^z, i \in \mathcal{V}$ denotes the vertical position of UAV $i$, $\tilde{p}_z$ is the relative position between leaders and the center of the constrained area in vertical planar. $k_{pl}^z$ and $k_{dl}^z$ are positive scalars.

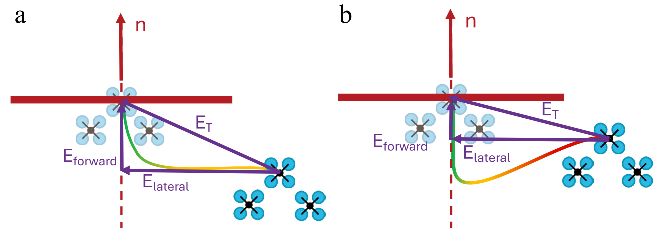


**Fig. 3** Diagram of leaders trajectory planning under normal and dangerous cases. (a) Trajectory planning under normal cases. (b) Trajectory planning when the leaders are seriously close to the constrained area but not aligned with the center of the area.

https://doi.org/10.48130/mav-0026-0012

## Collision-free controller

To ensure that multiple UAVs successfully achieve the desired formation, it is essential to implement an effective collision avoidance mechanism. According to the study by Guo et al.[23], the collision avoidance controller for UAV $i$ is designed as follows:

$$\begin{cases} u_i^c = -\sum\limits_{j\in N_i} k_p^c p_{ij}^c - k_v^c(\dot{p}_i^{xy} - \dot{p}_j^{xy}), \\ p_{ij}^c = \dfrac{1}{(\|p_i^{xy} - p_j^{xy}\| - r_s^c)^2}\dfrac{p_i^{xy} - p_j^{xy}}{\|p_i^{xy} - p_j^{xy}\|}, \end{cases} i \in \mathcal{V}, \tag{31}$$

where, $k_p^c, k_v^c$ are the positive gains, and $r_s^c$ is a positive scalar denoted as the safe distance among the UAVs. The stability analysis of the controller (31) has been addressed in reference[23], and a detailed discussion is omitted.

## Applications to quadcopters

The dynamics of a quadrotor system is typically characterized through the Newton–Euler formulation for rigid body motion, which provides a fundamental framework for platform stabilization and control. The dynamics of a quadrotor can be described as[24]:

$$\begin{bmatrix} \ddot{x} \\ \ddot{y} \\ \ddot{z} \end{bmatrix} = \begin{bmatrix} 0 \\ 0 \\ -g \end{bmatrix} + \frac{1}{m}\begin{bmatrix} -\sin\theta \\ \cos\theta\sin\varphi \\ \cos\theta\cos\varphi \end{bmatrix} f, \tag{32}$$

where, $x, y, z$ is the position of mass of the quadrotor, $\theta, \varphi$ is the eular angle of the quadrotor, and $f$ denotes the thrust.

For the typical configuration of a quadrotor, there is an autopilot onboard that controls its stability while following horizontal velocity commands given by an external position controller, shown in Fig. 4. In addition, to implement the vertical controller, compared with (32) and (8), we can design the desired thrust as:

$$f_i^d = \frac{g - u_i^z}{\cos\varphi_i \cos\theta_i}, i \in \mathcal{V}. \tag{33}$$

# Numerical simulation

To address the improvement of formation cohesion, transient response, and steady-state accuracy in quadrotors, we provide a numerical simulation example to validate the effectiveness of our method. Also, a comparison between the proposed approach of this paper and the approach introduced in reference[18] is made in this section. To validate the performance of the algorithm under real quadcopter dynamics, we used the first-order plus time-delay (FOTD) model to identify the velocity loop in DJI Tello drones. The identified model is considered for simulation and described as:

$$\frac{V(s)}{V_d(s)} = \frac{0.9889}{0.4899s + 1}\mathrm{e}^{-0.1s}. \tag{34}$$

Three cases are conducted in this section, as shown in Table 1. Case 1 demonstrates the performance improvement in the position control by utilizing historical velocity commands. Case 2 illustrates that the utilization of historical information significantly enhances the performance of the quadrotor altitude control. Case 3 verifies that the formation successfully completes the task of crossing different door frames. The simulation verifies that the proposed formation control strategy enables the group to navigate through various obstacles rapidly. The nominal framework is shown in Fig. 5, where orange nodes represent the leader and white nodes indicate the followers. This ensures that the formation can maintain a line-type following structure without altering the topological relationships.

## Simulation case 1

The simulation verifies the performance improvement achieved by introducing HHVC in position control. In this scenario, a door frame is constructed at the same altitude as the quadrotors, meaning that each quadrotor only needs to adjust its horizontal position to reach the desired location. The leader's trajectories are set to maneuver through the door frame, while the followers must converge to the nominal formation to jointly cross the target door frame. In this scenario, the follower formation control convergence performance is compared under both active and inactive historical velocity commands. The parameters are as follows:

$$\begin{aligned} &k_f = 1, k_c = 0.1, \tau = 0.02, k_\alpha = 0.17, k_\beta^{xy} = 1.25, \\ &\text{without HHVC: } k_f = 1, k_c = 0.1, k_p = 0.17, k_\beta^{xy} = 1.25. \end{aligned} \tag{35}$$

Figure 6 shows snapshots of the initial and terminal states, 3D trajectories, and tracking errors, with parameters. Note that the initial states are equivalent. Figure 6a illustrates a bad crossing task due to a lack of cohesion. In contrast, Fig. 6b demonstrates that the introduction of HHVC enhances cohesion in formation maneuver control, enabling successful completion of the crossing task. The comparison of cohesiveness is summarized in Table 2.

## Simulation case 2

This simulation aims to verify the performance improvement achieved by using historical acceleration commands in altitude control. A door frame is set up in the simulation environment, where

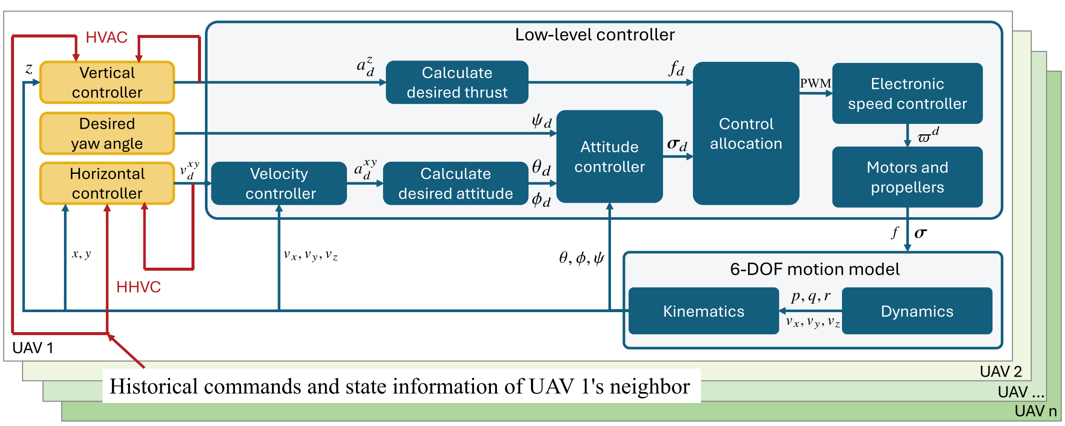


**Fig. 4** Designed vertical and horizontal controllers applied to the quadrotor with a low-level controller. Note that the paper is not concerned with yaw planning, and we set the desired yaw angle to zero.

**Table 1.** Simulation cases and purposes.

| Case | The purpose of the experiment cases |
|---|---|
| Case 1 | To verify the HHVC improves the performance in position control |
| Case 2 | To verify the HAC improves the performance in altitude control |
| Case 3 | To verify the adaptivity of the controller to diverse maneuvers |

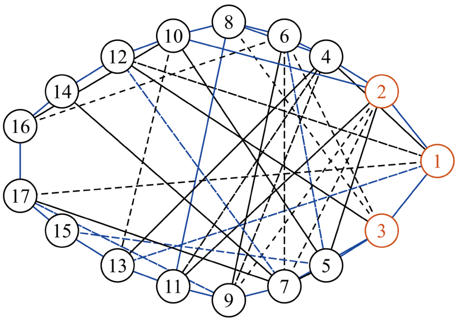


**Fig. 5** The nominal framework in simulation. Orange nodes indicate leaders and white nodes indicate followers. Solid lines represent positive stress while dashed lines denote negative stress. All lines are used for communication in the original network (47 edges), and blue lines are used in the line-type network (24 edges). $P(r)$ is the initial position.

the leader adjusts its altitude to complete the maneuvering task of crossing the door frame. The follower must perform altitude tracking control to ensure that the quadrotors cross the target safely. This simulation compares the altitude control performance with and without the introduction of historical acceleration commands. The parameters are as follows:

$$\begin{aligned} &k_p = 0.9, k_v = 2.0, \tau = 0.02, k_\beta^z = 1.0, \\ &\text{without HHAC: } k_p = 0.9, k_v = 2.0, k_\beta^z = 1.0. \end{aligned} \tag{36}$$

The simulation results are presented in Fig. 7. More specifically, Fig. 7 shows quadrotor trajectories and tracking errors. In this case, Fig. 7a shows a collision during the crossing task, indicating that insufficient cohesion in altitude control can lead to task failure. Figure 7b demonstrates that the quadrotors successfully cross the door frame quickly and safely by using historical acceleration commands. To further compare the improvement in cohesion performance, we evaluate the cohesion with and without HAC, which are summarized in Table 2.

## Simulation case 3

The purpose of this simulation is to verify the capability of the proposed controllers in a complex multi-frame crossing task. We set up several door frames of varying sizes, altitudes, and headings in the simulation environment. The group of quadrotors must maneuver through all the door frames rapidly and safely, relying on both position and altitude controllers proposed in this paper. In this simulation, the parameters for position control and altitude control are as follows:

$$\begin{aligned} &\text{HHVC: } k_f = 1, k_c = 0.1, \tau = 0.02, k_\alpha = 0.17, k_\beta^{xy} = 1.25, \\ &\text{HVAC: } k_p = 0.9, k_v = 2.0, \tau = 0.02, k_\beta^z = 1.0. \end{aligned} \tag{37}$$

The crossing process of the formation is illustrated in Fig. 8, which provides the top view of different crossing moments for frames. The three-dimensional trajectories of the quadrotors are shown in Fig. 8b. From the trajectory simulation results, we observe the following: (i) When passing through the second door frame, the

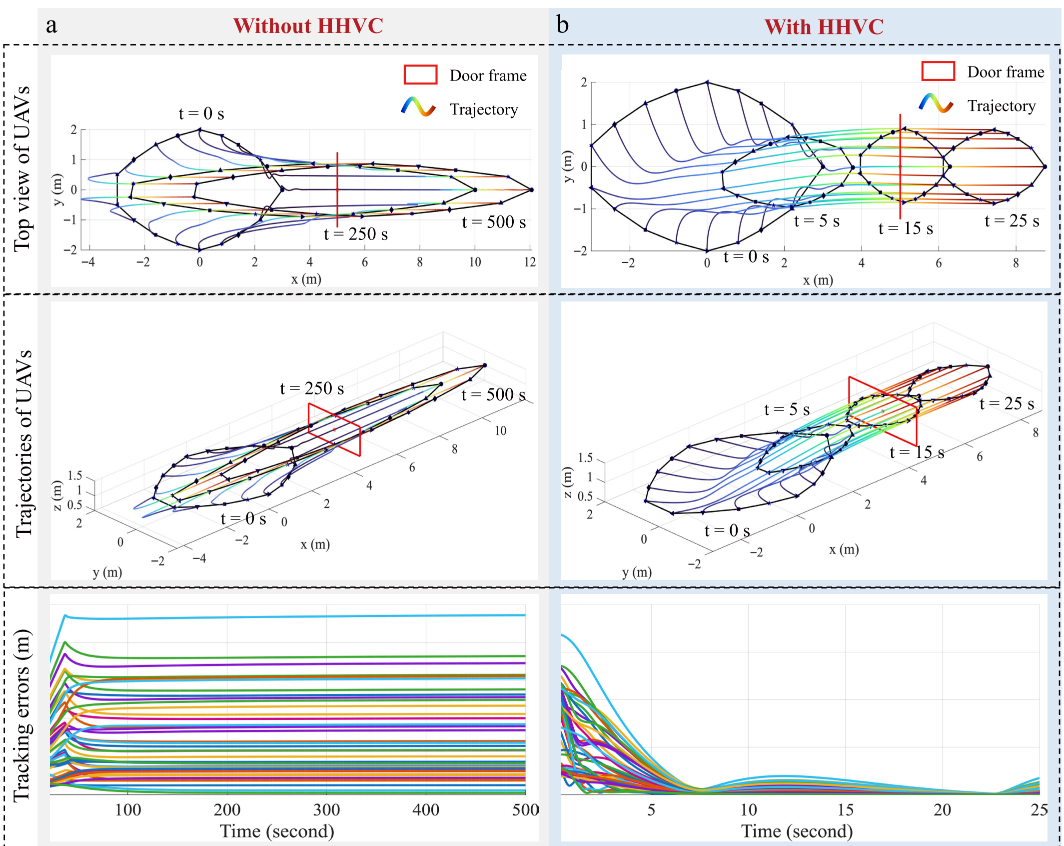


**Fig. 6** Simulation case 1. (a) Top view, trajectories, and error dynamics without HHVC in position control. (b) Top view, trajectories, and error dynamics with HHVC in position control.

https://doi.org/10.48130/mav-0026-0012

**Table 2.** Lack of cohesiveness $\Delta_f$ in three different cases in simulations.

| Channel | Case 1 | | Case 2 | | Case 3 |
|---|---|---|---|---|---|
| | Without HHVC | With HHVC | Without HVAC | With HVAC | |
| Position (x) | Unsettled | 2.58 | / | / | 2.34 |
| Position (y) | Unsettled | 0.99 | / | / | 0.84 |
| Altitude (z) | / | / | 0.74 | 0.019 | 0.02 |

formation switches to a line-type formation to complete the crossing due to its narrow width. (ii) When passing through the fifth door frame, the safe distance between formation members increases, which is relatively wide. (iii) When facing the last door frame, the formation contracts slightly to ensure safe passage. These observations demonstrate that the controller, based on historical command information, effectively ensures the cohesion of a group of quadrotors under control.

# Experiments

To verify the improvement in the formation cohesiveness and traversability, real indoor experiments have been conducted on a group of seven DJI Tello quadcopters (Fig. 9a). The topological relation of seven DJI Tello quadcopters is shown in Fig. 10. Two experiments are considered and the scenario design is shown as Fig. 9b. The first experiment is to verify the significant improvement in formation cohesiveness and the enhancement of swarm UAV traversability following the integration of historical commands. The second experiment is to verify the performance and traversability of the proposed method.

## Experiment case 1

***Comparing the traversability of formation scaling strategies with and without the HHVC***

From Fig. 11, the formation controller without HHVC has a large formation tracking error and causes a collision while travelling the constrained area. From Fig. 12, the formation controller with HHVC is more cohesive and successfully traverses the constrained area without any collision. From Table 3, we can learn that the formation controller with HHVC is more cohesive than the one without HHVC. Based on the results, we conclude that the introduction of HHVC improves the cohesiveness and the traversability of the UAV swarm.

## Experiment case 2

***Comprehensive formation traversable maneuver in multiple constrained areas***

From Fig. 13a, the UAV swarm successfully traverses all gates with different heights and orientations. From Fig. 13b, the horizontal formation tracking error converges rapidly while maneuvering. From Fig. 13b, the vertical formation tracking error remains small throughout the whole flight because the acceleration command generated by the vertical formation controller possesses higher dynamic response capability for drones. Besides, the mean lack of cohesion of $\Delta_f$ of the traversing formation task in three axis are $\overline{\Delta_f^x} = 0.292, \overline{\Delta_f^y} = 0.205, \overline{\Delta_f^z} = 0.111$, respectively, which indicates the cohesiveness of the drone swarm is quite strong.

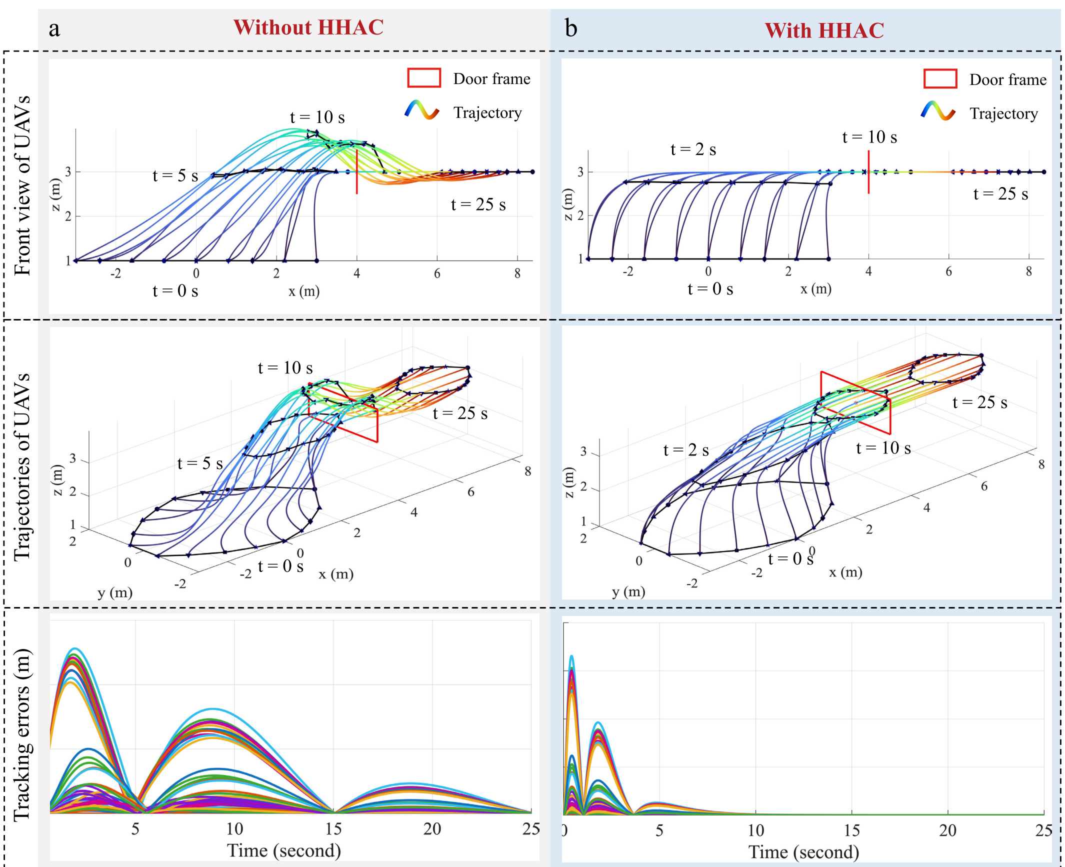


**Fig. 7** Simulation case 2. (a) Front view, trajectories, and error dynamics without HHAC in altitude control. (b) Front view, trajectories, and error dynamics with HHAC in altitude control.

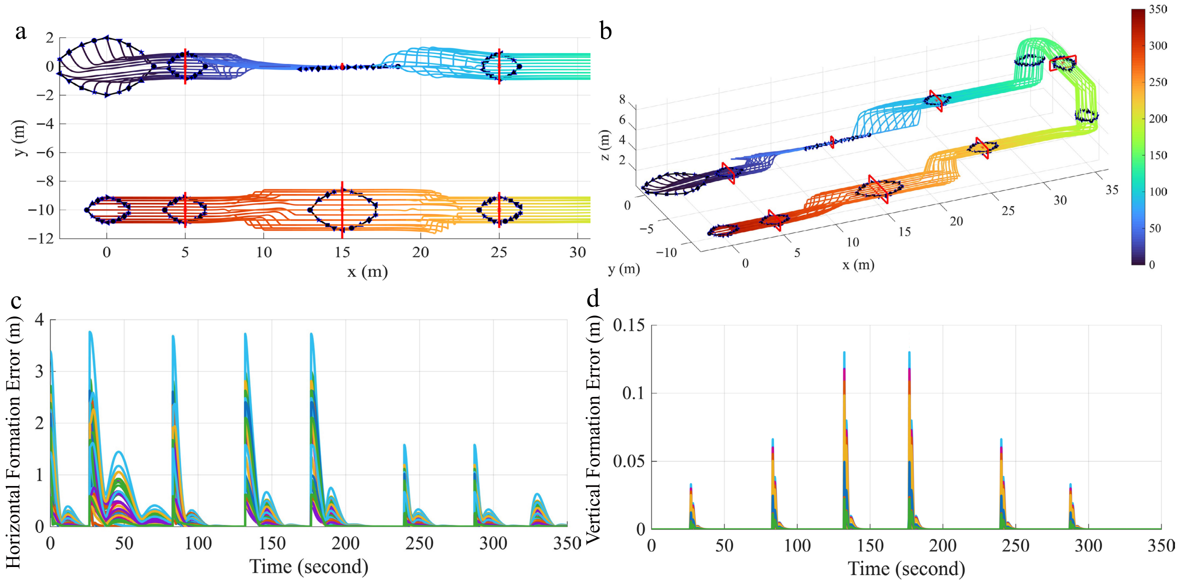


**Fig. 8** Simulation case 3. (a) Top and 3D views of quadrotor swarms trajectories; (b) formation tracking errors in position control; (c) formation tracking errors in altitude horizontal control; (d) formation tracking errors in altitude control.

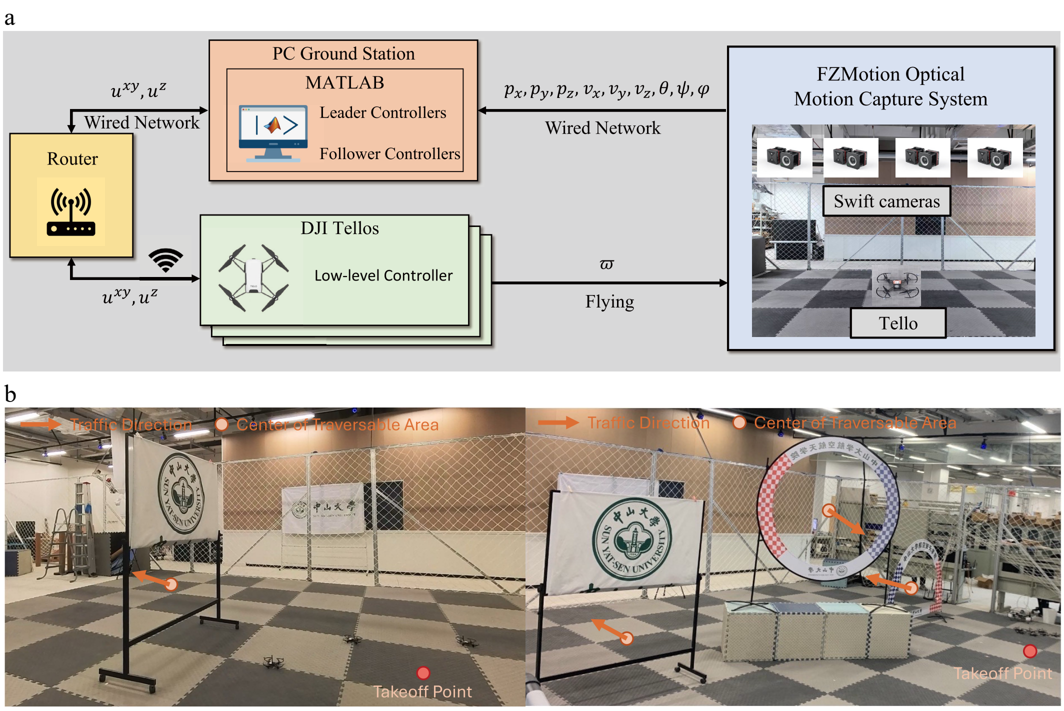


**Fig. 9** Experimental setup. (a) Diagram of communication topology, signal flow and experiment platform. Note that our proposed distributed algorithm was experimentally verified using a centralized communication infrastructure. (b) Snapshots of experiments scenario setup. The Left one is for the experiment 1, and the right one is for the experiment 2.

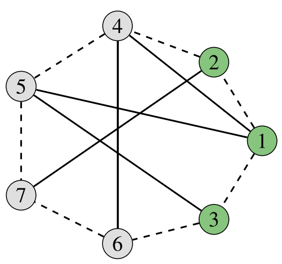


$$P(p^{*xy}) = \begin{bmatrix} 1.2 & -0.15 \\ 0.8 & 0.5 \\ 0.8 & -0.8 \\ 0.0 & 0.8 \\ -0.8 & 0.3 \\ 0.0 & -1.0 \\ -0.8 & -0.6 \end{bmatrix}$$

**Fig. 10** Nominal formation based on an undirected graph in the experiment. Green nodes represent the leaders. $P(p^{*xy})$ is the vector of positions of the nominal formation framework.

The experimental results demonstrate that our proposed method enhances both the cohesiveness and traversability of the drone swarm formation, enabling the effective and secure traversal of constrained regions with rapid task completion.

# Conclusions

This paper proposed a new approach based on an enhanced affine formation maneuver control for a swarm of quadrotors to traverse multiple gates. The target formation is a time-varying affine

https://doi.org/10.48130/mav-0026-0012

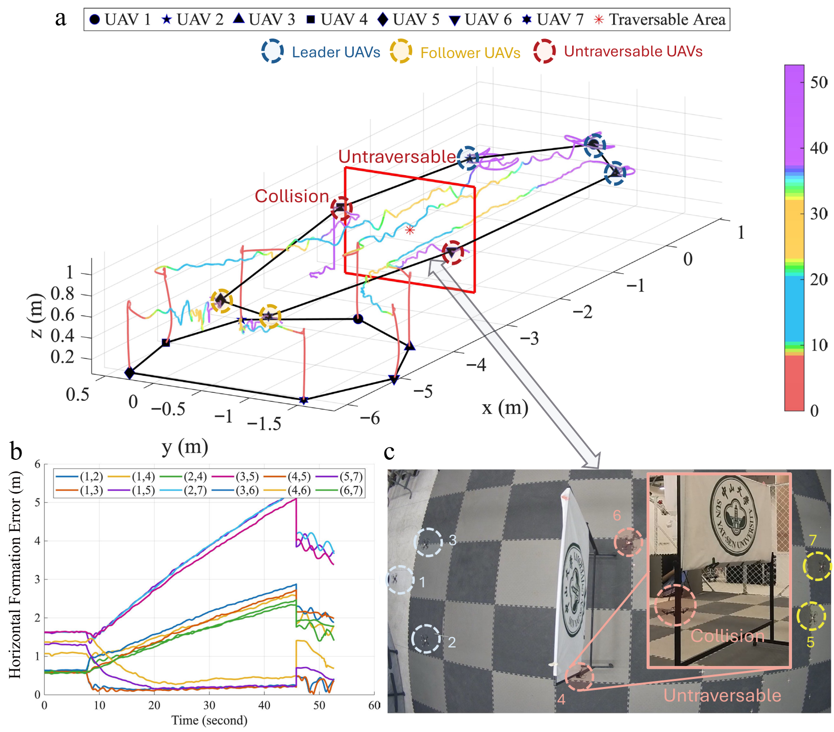


**Fig. 11** Experiment 1: Traversing task using the controller without HHVC. (a) The complete trajectory of the travel task and the traversability of the UAV swarm. (b) The formation tracking error of the UAV swarm. (c) The snapshot of a UAV swarm traveling in the constrained area.

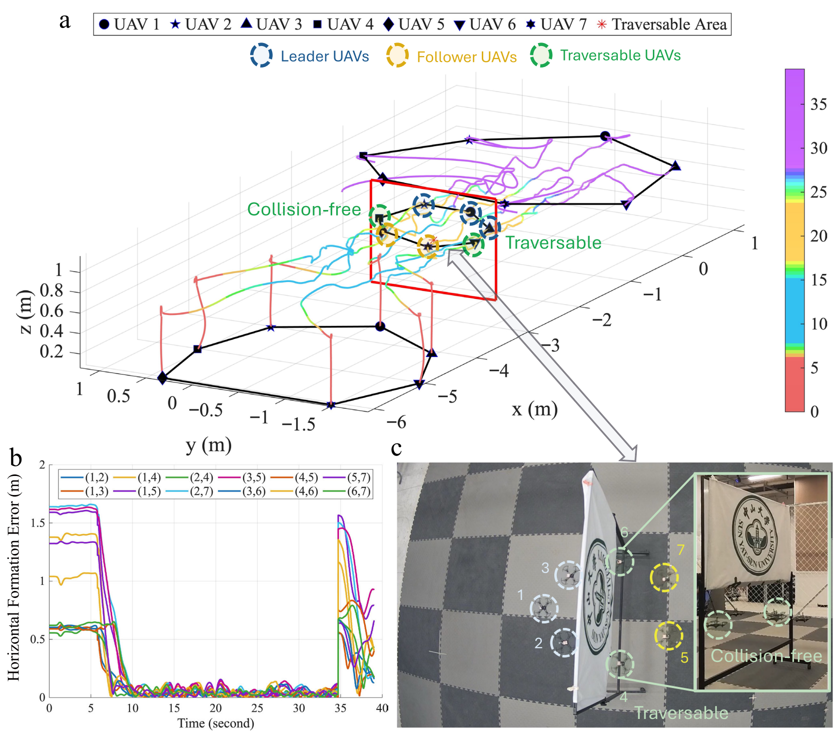


**Fig. 12** Experiment 1: Traversing task using the controller with HHVC. (a) The complete trajectory of the travel task and the 3D traversability of the UAV swarm. (b) The formation tracking error of the UAV swarm. (c) The snapshot of the UAV swarm traveling in the constrained area. $(k_\omega^{xy} = 0.8, k_\kappa = 1, k_p^{xy} = 0.83)$.

transformation of a nominal formation, and the two types of formation maneuver, rotation and scaling, are mainly considered. The distributed control laws for follower quadrotors, which actively use the historical control commands for single-integrator and double-integrator, are proposed to improve the formation tracking performance in horizontal and vertical channels. We also propose a method to generate scaling and rotation control commands for the leaders. We consider the flight task of traversing three gates with

**Table 3.** Lack of cohesiveness $\Delta_f$ in Experiment case 1.

| HHVC | Cohesiveness $\Delta_f$ | |
|---|---|---|
| | x-axis | y-axis |
| Without | Unsettled | 0.723 |
| With | 1.053 | 0.287 |

diverse altitude and directional configurations to evaluate the proposed algorithms on a swarm of seven DJI Tello quadrotors. Both numerical simulations and physical experiments demonstrate the efficacy of the proposed method, characterized by rapid transient response, high-fidelity tracking, and robust traversability through diverse gate configurations.

Future work includes two aspects: (1) theoretically analyzing the performance of the closed-loop system by incorporating identified autopilot models; and (2) robustness optimization of onboard perception, planning, and control algorithms.

## Author contributions

The authors confirm their contributions to the paper as follows: conceptualization and writing—original draft: Yi P; validation: Xie J, Yu W; software development: Xie J; methodology: Yu W, Zhu B; review and editing: Zhu B, Hu T, Huang D. All authors reviewed the results and approved the final version of the manuscript.

## Data availability

The datasets generated during and/or analyzed during the current study are available from the corresponding author on reasonable request.

## Acknowledgments

This work was supported in part by the National Key Research and Development Program of China under Grant No. 2024YFC3015801; in part by the National Natural Science Foundation of China under

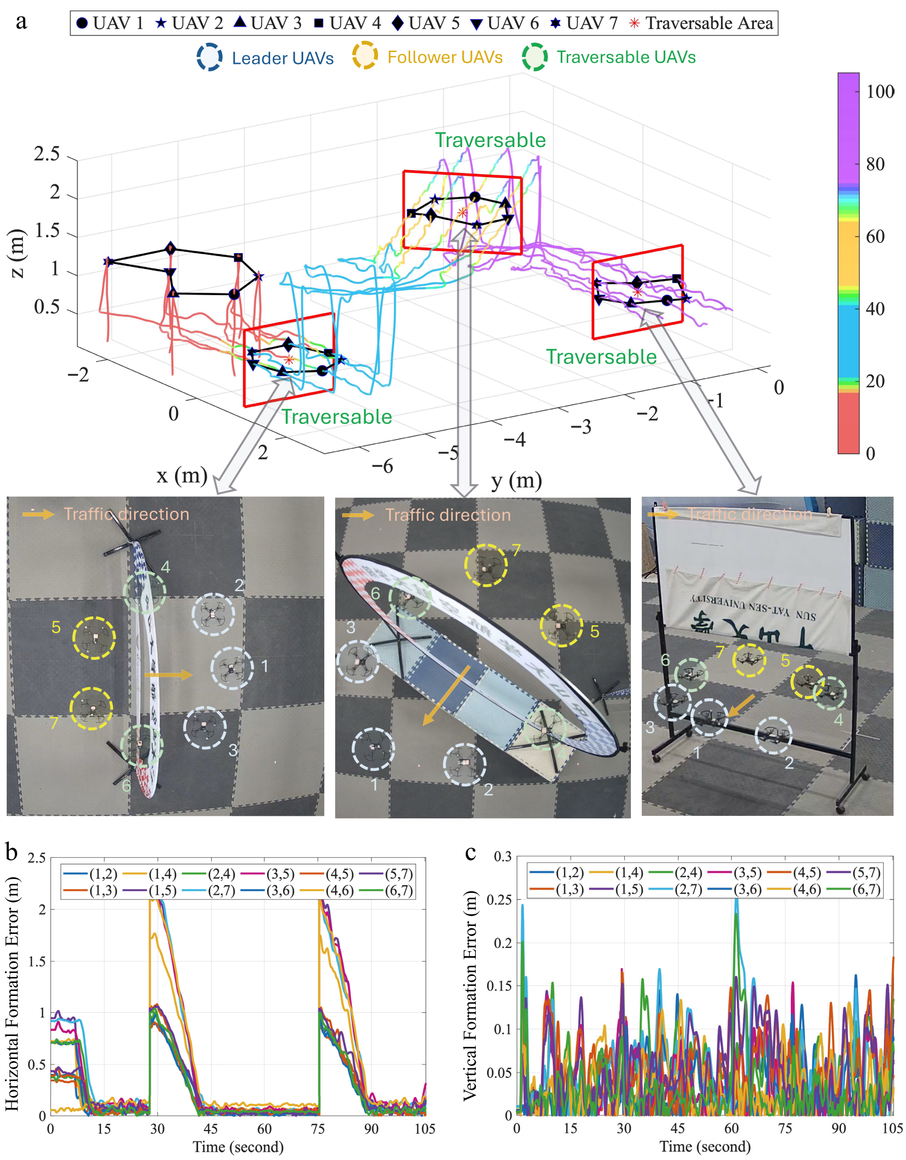


**Fig. 13** Experiment 2: Comprehensive formation traversable maneuver under multiple limited traversable areas with controller (11). (a) Complete trajectory and traversable formation in complex limited areas with three snapshots of traveling the different constrained areas. (b) Horizontal formation tracking error. (c) Vertical formation tracking error.

https://doi.org/10.48130/mav-0026-0012

Grant No. 62373386; and in part by the China University Industry-University-Research (IUR) Innovation Fund under Grant No. 2024ZY006.

## Conflict of interest

The authors declare that they have no conflict of interest.

## Dates

Received 25 March 2026; Revised 10 May 2026; Accepted 25 May 2026; Published online 17 September 2026

## References

[1] Zhu F, Ren Y, Yin L, Kong F, Liu Q, et al. 2025. Swarm-LIO2: decentralized efficient LiDAR-inertial odometry for aerial swarm systems. *IEEE Transactions on Robotics* 41:960–981
[2] Monwar M, Semiari O, Saad W. 2018. Optimized path planning for inspection by unmanned aerial vehicles swarm with energy constraints. *2018 IEEE Global Communications Conference (GLOBECOM), Abu Dhabi, United Arab Emirates, 2018*. Abu Dhabi, United Arab Emirates: IEEE. pp. 1–6 doi: 10.1109/GLOCOM.2018.8647342
[3] Albanese A, Sciancalepore V, Costa-Pérez X. 2022. SARDO: an automated search-and-rescue drone-based solution for victims localization. *IEEE Transactions on Mobile Computing* 21(9):3312–3325
[4] Chen L, Mei J, Li C, Ma G. 2020. Distributed leader–follower affine formation maneuver control for high-order multiagent systems. *IEEE Transactions on Automatic Control* 65(11):4941–4948
[5] Lin Z, Wang L, Chen Z, Fu M, Han Z. 2016. Necessary and sufficient graphical conditions for affine formation control. *IEEE Transactions on Automatic Control* 61(10):2877–2891
[6] Zhao S. 2018. Affine formation maneuver control of multiagent systems. *IEEE Transactions on Automatic Control* 63(12):4140–4155
[7] Li D, Ma G, Xu Y, He W, Ge SS. 2021. Layered affine formation control of networked uncertain systems: a fully distributed approach over directed graphs. *IEEE Transactions on Cybernetics* 51(12):6119–6130
[8] Wang J, Ding X, Wang C, Liang L, Hu H. 2021. Affine formation control for multi-agent systems with prescribed convergence time. *Journal of the Franklin Institute* 358(14):7055–7072
[9] Xiao F, Yang Q, Zhao X, Fang H. 2022. A framework for optimized topology design and leader selection in affine formation control. *IEEE Robotics and Automation Letters* 7(4):8627–8634
[10] Yu W, Yi P, Zhu B, Liu H, Hu T. 2023. Enhanced affine formation maneuver control using historical acceleration command. *International Journal of Robust and Nonlinear Control* 33(18):11458–11480
[11] Yu W, Zhu B, Wang X, Yi P, Liu H, et al. 2023. Enhanced affine formation maneuver control using historical velocity command (HVC). *IEEE Robotics and Automation Letters* 8(11):7186–7193
[12] Wang D, Pan Q, Hu J, Zhao C, Guo Y. 2019. MPCC-based path following control for a quadrotor with collision avoidance guaranteed in constrained environments. *2019 IEEE 28th International Symposium on Industrial Electronics (ISIE), Vancouver, BC, Canada, 2019*. Vancouver, BC, Canada: IEEE. pp. 581–586 doi: 10.1109/ISIE.2019.8781353
[13] Bonatti R, Madaan R, Vineet V, Scherer S, Kapoor A. 2020. Learning visuomotor policies for aerial navigation using cross-modal representations. *2020 IEEE/RSJ International Conference on Intelligent Robots and Systems (IROS), Las Vegas, NV, USA, 2020*. Las Vegas, NV, USA: IEEE. pp. 1637–1644 doi: 10.1109/IROS45743.2020.9341049
[14] Cyba A, Szolc H, Kryjak T. 2021. A simple vision-based navigation and control strategy for autonomous drone racing. *2021 25th International Conference on Methods and Models in Automation and Robotics (MMAR), Międzyzdroje, Poland, 2021*. Międzyzdroje, Poland: IEEE. pp. 185–190 doi: 10.1109/MMAR49549.2021.9528463
[15] Devasia S. 2020. Cohesive networks using delayed self reinforcement. *Automatica* 112:108699
[16] Attanasi A, Cavagna A, Del Castello L, Giardina I, Grigera TS, et al. 2014. Information transfer and behavioural inertia in starling flocks. *Nature Physics* 10(9):691–696
[17] Tiwari A, Devasia S, Riley JJ. 2023. Low-distortion information propagation with noise suppression in swarm networks. *Proceedings of the National Academy of Sciences of the United States of America* 120(11):e2219948120
[18] Yang Q, Sun Z, Cao M, Fang H, Chen J. 2019. Stress-matrix-based formation scaling control. *Automatica* 101:120–127
[19] Connelly R. 2005. Generic global rigidity. *Discrete & Computational Geometry* 33(4):549–563
[20] Toro-Arcila CA, Becerra HM, Arechavaleta G. 2025. Monocular visual servo control of a quadcopter for crossing windows, doors, and corridors. *Asian Journal of Control* 27(6):2706–2723
[21] Tang Z, Cunha R, Cabecinhas D, Hamel T, Silvestre C. 2021. Quadrotor going through a window and landing: an image-based visual servo control approach. *Control Engineering Practice* 112:104827
[22] Li S, Ozo MMOI, De Wagter C, de Croon GCHE. 2020. Autonomous drone race: a computationally efficient vision-based navigation and control strategy. *Robotics and Autonomous Systems* 133:103621
[23] Guo J, Qi J, Wang M, Wu C, Ping Y, et al. 2022. Collision-free formation tracking control for multiple quadrotors under switching directed topologies: theory and experiment. *Aerospace Science and Technology* 131:108007
[24] Das A, Subbarao K, Lewis F. 2009. Dynamic inversion with zero-dynamics stabilisation for quadrotor control. *IET Control Theory & Applications* 3(3):303–314